A critical comparison of several numerical methods for computing effective properties of highly heterogeneous materials

Cyrille F. Dunant [f,*], Benoît Bary [a], Alain B. Giorla [g], Christophe Péniguel [b], Julien Sanahuja [c], Charles Toulemonde [c], Anh-Binh Tran [c,e], François Willot [d], Julien Yvonnet [e]

[a] CEA, DEN, DPC, SECR, Laboratoire d'Etude du Comportement des Bétons et des Argiles, F-91191 Gif-sur-Yvette, France
[b] EDF R&D/MFEE Department – 6, quai Watier, BP 49, F-78401 Chatou cedex, France
[c] EDF R&D/MMC Department – Site des Renardiéres, Route de Sens, Ecuelles, F-77250 Moret sur Loing, France
[d] École des Mines ParisTech/Centre de Morphologie Mathématique 35, rue Saint-Honoré, F-77305 Fontainebleau cedex, France
[e] Université Paris-Est, Laboratoire Modélisation et Simulation Multi-Echelle (MSME UMR CNRS 8208), 5 boulevard Descartes, F-77454 Marne La Vallée cedex, France
[f] University of Toronto, Galbraith Building, 35 St. George Street, Toronto, Canada M5S 1A4
[g] EPFL-STI-IMX-LMC, Station 12, CH-1015 Lausanne, Switzerland

ARTICLE INFO

ABSTRACT

Modelling transport and long-term creep in concrete materials is a difficult problem when the complexity of the microstructure is taken into account, because it is hard to predict instantaneous elastic responses. In this work, several numerical methods are compared to assess their properties and suitability to model concrete-like microstructures with large phase properties contrast. The methods are classical finite elements, a novel extended finite element method (μ-XFEM), an unconstrained heuristic meshing technique (AMIE), and a locally homogenising preprocessor in combination with various solvers (BENHUR). The benchmark itself consists of a number of simple and complex microstructures, which are tested with a range of phase contrasts designed to cover the needs of creep and transport modelling in concrete. The calculations are performed assuming linear elasticity and thermal conduction. The methods are compared in term of precision, ease of implementation and appropriateness to the problem type. We find that XFEM is the most suitable when the mesh if coarse, and methods based on Cartesian grids are best when a very fine mesh can be used. Finite element methods are good compromises with high flexibility.

© 2013 Elsevier Ltd. All rights reserved.

1. Introduction and literature background

Understanding the link between microstructural make-up and material properties is a central aspect of the study of composites. Concrete is the most used composite material in the world and is critical in civil engineering applications, notably for critical installations, such as nuclear plants. Furthermore, it is used for very long term applications, for example as a casing material for nuclear waste management. Understanding and predicting its mechanical behaviour is important for design, maintenance and diagnostic applications. Concrete is composed of aggregates following a continuous gradation curve which are embedded in a cement paste matrix. For simulation purposes, new tomography techniques have made it practical to obtain images of microstructures [1], or reconstructions based on gradation curves can be used as in the present work. However, making predictions on the mechanical properties of concrete from its mix design is still an open question [2]. Although the difficulties in this mostly come from the develop-

ment of the strength of the cement paste, the make-up of the composite remains a critical aspect of the question. This work focuses on the description of numerical homogenisation tools which can be used to derive material behaviour applicable to the simulation of structures.

The general problem of obtaining the apparent or homogenised properties of a composite from the mechanical properties of its constituents and their geometrical make-up can be approached in a number of ways. Analytical techniques, such as the Mori and Tanaka [3] and self-consistent schemes [4] can give good estimates. However these techniques are limited if the phase contrasts are too high or the morphology too complex. Furthermore, homogenisation schemes such as the Mori–Tanaka scheme are not appropriate for large inclusion volume fractions (above 30–40%) [5,6]. Progress has been made in the effective medium theory for periodic solids with respect to phase contrast [7]. However in concrete, although the phase stiffness contrast is fairly low for elastic applications, the sizes of aggregates span orders of magnitude with no scale separation. Further, when considering visco-elastic problems, the phase contrasts can be enormous. Numerical modelling using microstructures in representative elementary volumes (REV) is the

* Corresponding author.
E-mail address: cyrille.dunant@gmail.com (C.F. Dunant).

alternative approach when analytical methods fall short. The size of the REV as well as the importance of boundary conditions has been studied by Huet as well as by Kanit [8,9]. Indeed, explicit modelling of the microstructure is not a new approach [10–13], but it is not usually practical to model fully detailed geometry at the micro-scale in 3D and application-specific trade-offs are made [14]; even 2D simulations try to limit the number of represented aggregates as in [15].

In the case of concrete, a representative elementary volume is approximately 3–5 times the size of the maximum aggregate diameter [16]. Although it is in any case neither possible nor necessary to model every grain of sand in such a volume, it is still necessary to model the larger grains, which number in the thousands. The geometry can be produced by generating the aggregates artificially from statistical information [14,17], or from tomography data [18,1]. In a classical finite element approach, every grain must be meshed and the mesh must be verified for geometrical accuracy and refined near the interfaces. This yields extremely large number of elements. Therefore strategies have to be devised which, given constraints on the number of degrees of freedom, can best approximate the properties of real microstructures. When the microstructure is obtained from tomography, a voxel-based approach is natural, but this introduces important distortions at the interfaces and induces artificial anisotropy, as the normals to phase surfaces can only have three orientations.

Approximations are introduced by the numerical methods themselves. Numerical errors can come from the size of elements, which may be too large to properly represent the strain or flux gradients. Conforming adaptive meshes can double the convergence of the error with respect to element size [19], but are not practical with intrinsically multi-scale concrete geometries. If the number of degrees of freedom is limited, the boundaries between the phases are poorly approximated and if the solver requires Cartesian grids, the mesh might not be constrained to the microstructure at all. Adaptive strategies, notably regarding the time-step in transport of multiphysics problems have been used. This is notably the case in the work of Zodhi and colleagues [12,20]. Beyond errors due to high field gradients not being adequately captured, producing a non-conforming geometry can affect the results in a number of ways: artificial connection of disconnected grains, approximations of the boundaries of grains such that the volume fraction of the phases in the microstructure can be affected. These effects can significantly affect the apparent properties of the microstructure.

This paper presents a number of approaches developed independently as attempts to model concrete through its microstructure. To solve the problems highlighted above, different methods to generate and attribute phase behaviour to the elements are used. All the methods have in common that they attempt to reproduce the effect of the interfaces present in the input geometry. The well-established FEM method uses compact elements in which the phase is constant. Thus, the discretisation scheme is responsible for the accuracy of the representation of boundaries. To accurately reproduce the effect of complex interfaces passing through the elements, XFEM-based approaches introduce enrichment functions with discontinuous derivatives across the interface in the classical FEM approximation. BENHUR is a preprocessor which attributes homogenised behaviour to elements overlapping grains; it is tested in conjunction with a number of numerical methods on Cartesian grids. AMIE uses a hybrid approach: it uses a meshing heuristic to generate a mesh which follows as much as possible the geometrical boundaries imposed by the microstructure, but with a hard constraint on the number of degrees of freedom and not on the geometry. To compare the methods, a set of benchmarks were devised, and the results of theses novel approaches were compared to that of a classical finite element scheme.

The ability of the methods to recover apparent properties are tested with both a steady-state transport problem and a linear elastic one with homogeneous boundary conditions. Indeed non-linear problems can only be considered once the linear case is well understood. The input microstructures have perfect interfaces, and the numerical difficulty of the problem come from the geometric complexity and the high phase contrasts. The precision reached for each of the methods is reported as a function of the typical element size. The benchmark tests are first described in detail, then the results are presented and discussed.

2. Description of the tests

The general behaviour of the numerical methods is first established using microstructures consisting in a single sphere or octahedron in the volume. The sphere set-up has no geometrical singularities, and reflects the convergence of the numerical method, rather than the convergence of the errors due to geometrical approximations. It also highlights the difference between methods allowing curved surfaces on their elements, such as the FEM when using quadratic elements with intermediate nodes projected on the sphere surface. The sharp edges of the octahedron highlight how the presence of stress or flux concentrators affect the precision of the simulations, although its edges and vertices are rounded in the μ-XFEM approximation, due to the usage of level-sets. Both the octahedron and the sphere serve as proof of concept for those methods which use homogenised elements such as BENHUR, or level sets to describe geometries, such as XFEM, as the underlying Cartesian grids converge to the exact geometries as they are refined.

The core of the benchmark is the simulation of concrete- and mortar-like microstructures. The first microstructure, "B11", is designed for simulations assuming periodic boundaries. It is composed of 2024 spheres with a size distribution resembling that of concrete. These spheres are well separated, but overlap the volume boundaries. The second "B3200" is a mortar-like microstructure, where all the spheres are confined within the volume. The repulsion distance in this later microstructure is much lower, which makes its simulation more sensitive to errors in the discretisation of the aggregate boundaries. The results presented here have been rescaled so that the box has a side length of 1. The geometries used are illustrated in Fig. 1.

The phase fractions as well as the essential parameters of the geometries are reported in Table 1. All microstructures have similar phase ratios. The concrete has an aggregate volume fraction of approximately 40%, indicating that approximately only half the volume of aggregates which would have been present in a real concrete are represented. The same is true for the mortar: a complete microstructure would have a volume fraction around 65%. However, Concrete and mortar are not 2-phase materials, and the interface transition zone as well as the macro-pores have been shown to affect the mechanical properties of the composite. These are not considered in this study which focuses on the properties of the numerical tools described. These results can be nonetheless extended to more complex, multi-phase materials which more closely correspond to the real ones.

As well as testing the effect of complex geometries on numerical approximations, the benchmark is designed to assess how the various methods behave when the phase contrast between the physical properties of the inclusions and the matrix is high. The relative properties are reported in Table 2. The moderate contrast in the elastic case corresponds roughly to real concrete, whereas the high case has been chosen to anticipate the needs of creep homogenisation [21]. The thermal contrasts cover an extreme range of physically plausible values.
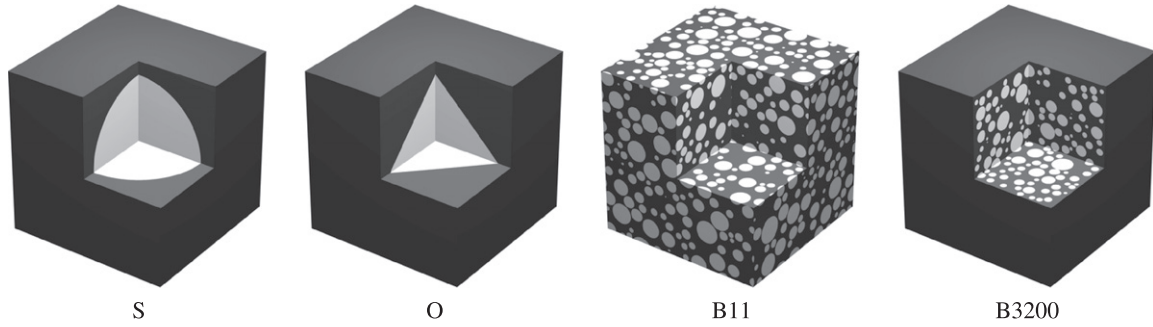
Fig. 1. Illustration of the four microstructures used in the benchmark: the single sphere, the single octahedron, the prediodic concrete and the mortar cube.

Table 1
Essential phase information about the microstructures. f_i the inclusion fraction, $\varnothing_{min}$ the minimum diameter, $\varnothing_{max}$ the maximum diameter and d_{min} the minimum inter-inclusion distance.

	# Inc.	f_i	$\varnothing_{min}$	$\varnothing_{max}$	d_{min}
S	1	0.300	0.620		–
O	1	0.100	0.837		–
B11	2024	0.402	0.043	0.167	1.14×10^{-3}
B3200	3200	0.361	0.036	0.125	2.17×10^{-7}

Table 2
Relative physical properties of the matrix and inclusions, E_i and E_m the Young's moduli of the inclusion and matrix respectively; similarly v the Poisson ratio and λ the conductivity.

	Mechanical			Thermal
	E_i/E_m	v_i	v_m	λ_i/λ_m
Low contrast	10^{-8}	0.2	0.2	10^{-2}
Moderate	3	0.4	0.1	–
High contrast	10^2	0.2	0.2	10^2

The very low stiffness (10^{-8}) simulates pores rather than inclusions and can be considered to demonstrate the abilities of the various algorithms to deal with foam-like structures. Furthermore, there are effectively pores in the microstructure of concrete, and the test of the methods with such a large void fraction can be seen as validation for the establishment of a homogenised model of paste and pores.

Two types of boundary conditions are tested, Dirichlet and Neumann (Fig. 2). In mechanical simulations, either a homogeneous displacement or a homogeneous stress was applied to the computational volumes along the first axis. Similarly, in the thermal cases, a homogeneous temperature gradient and homogeneous heat flux were applied. As those boundary conditions are inapplicable for FFT solvers, only periodic boundary conditions were applied in the latter case.

3. Numerical methods

3.1. FEM baseline

The baseline results were obtained using CAST3M [1] The mesh was generated using the tools provided by the SALOME[2] platform, which was used previously to generate cement microstructures [22]. The mesh properties are reported in Table 3. The meshes generated using these methods are conforming: the element faces are constrained to

have their vertices lie on the inclusion faces. The mechanical calculations were performed using CAST3M, which employs a parallel Krylov solver. The larger meshes took up to 10 h to converge on a workstation. This illustrates the need to develop efficient numerical methods for the calculation of apparent properties as a straight finite element strategy is very costly. Coarser meshes cannot be obtained as there is a constraint on the number of nodes used to represent a sphere.

Mesh sensitivity analysis was then performed using the SYRTHES[3] [23,24] code. The mesh was refined twice using a splitting strategy, leading to a very large mesh of 1.496 billion elements (the size of the geometry mesh file handled by SYRTHES is around 108 Gb). The thermal problem was then solved for each successive refinement. This showed that the baseline obtained from the finite element calculations is relatively close to the final values (Table 4).

3.2. Heuristic meshing and FEM

AMIE has been developed as a generic FEM/XFEM platform, and was designed to model concrete at the microstructure level [25,17,26]. The mesher used does not enforce strict geometric conformance, but rather is designed to generate a mesh which is good enough assuming the following assumptions are true:

1. The density of sampling points is homogeneous throughout the mesh.
2. Exact geometric representation is not required.

These assumptions are reasonable for concrete, as the phase contrast is moderate—but this is not true in all the benchmark test presented in this work—and therefore similar mesh density is required in aggregates and in paste, and microstructures are not exact but specified as particle size distributions. The node distribution on each sphere surface is computed for each sphere individually:

1. points are placed at random on the sphere surface,
2. they are given an acceleration based on their proximity to all other points,
3. all points are displaced and re-projected on the sphere surface, and
4. a specified number of iterations of this process are effected

The result of this algorithm is a very homogeneous point density, which makes the best use of the nodes available for discretisation. The mesher integration is also used to accelerate the computing of damage [27].
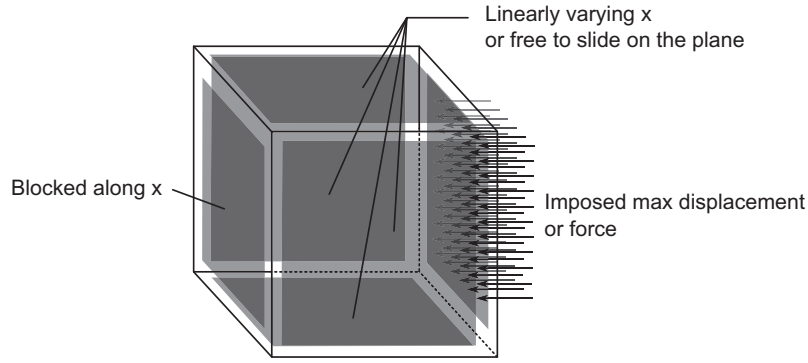

Fig. 2. The boundary conditions are established by restricting the x displacement on the bottom plane, by imposing planar displacements on the sides. In the case of homogeneous displacement linearly varying x displacements are further imposed and in the case of homogeneous force, it is applied on the plane opposite to the bottom.

Table 3
Number of elements in the conforming finite element meshes used for the mechanical tests.

Sphere	Octahedron	B11 concrete	mortar
Millions of elements			
0.732	1.12	16.1	10.1

Table 4
Mesh sensitivity around the baseline meshes, for the diffusion problems, on the B11 morphology.

Elements ($\times 10^6$)	23.4	187	1496
Cores	8	64	256
λ_{eff}	6.0671	5.9424	5.8963
Time (s)	174	1380	4232

Each geometric feature of the mesh is individually sampled. Then, the nodes present in overlapping geometries are removed. Finally, the node set is given as an input to a Delaunay mesher. As the meshed elements resulting from this procedure are not necessarily fully contained in a single feature, their mechanical or transport properties are determined by the location of their centres. A better homogenisation scheme could improve the results, but has not been implemented. The benefit of introducing such a scheme can be inferred from the BENHUR approach described below.

As the mesh density is fixed, smaller features may not be represented. The heuristic however ensures that the phase content remains close to the specification. This is because the attribution of phase properties to elements behaves like random point sampling inside the volume. If smaller features are known to be important and need explicit representation, this can be done using XFEMS.

3.3. XFEM/levelset method

The XFEM (Extended Finite Element Method) is a versatile method to accurately describe complex interfaces in non-conforming (possibly regular) meshes. In the context of the present problem, meshing 3D complex interfaces induces high computational costs. In contrast, the XFEM [28–32] is based on the enrichment of the finite element approximation with additional functions that model interfaces or singularities independently of the background mesh. The method has been successfully applied for the homogenization of microstructures [31]. Nevertheless, in the case of high volume fractions and nearby inclusions, it has been shown that the classical XFEM/level-set method induces several artefacts, leading to a low convergence of both local and effective fields with respect to the

mesh size [33]. In the present paper, we use a modified version of XFEM called μ-XFEM, which can handle the complex microstructures related to the benchmark test cases geometries [33]. In μ-XFEM, each inclusion is associated with a dedicated level-set function (cf. Fig. 3). The μ-XFEM displacement approximation is given below as a sum of FEM and XFEM terms:

$$\mathbf{u}^h(\mathbf{x}) = \sum_{i \in \mathscr{S}} N_i(\mathbf{x})\mathbf{u}_i + \sum_{k}^{N_{\text{int}}} \sum_{j \in \mathscr{S}^{ek}} N_j(\mathbf{x})\psi^k(\phi^k(\mathbf{x}))\mathbf{a}_j^k \qquad (1)$$

where $\mathbf{a}_j^k$ are nodal unknowns, the nodal set $\mathscr{S}^{ek}$ is defined as $\mathscr{S}^{ek} = \{j | j \in \mathscr{S}, \omega_j \cap \Gamma^k \neq 0\}$ and $\psi^k(\phi^k(\mathbf{x}))$ is an enrichment function constructed via the level-set functions ϕ^k of inclusion k with boundary Γ^k. The general level-set function ϕ^k takes the following form:

$$\Gamma_k = \{\mathbf{x} \in \mathbb{R}^d | \phi^k(\mathbf{x}) = 0\} \qquad (2)$$

In the case of spherical inclusions, the level-set function takes the form:

$$\phi^k(\mathbf{x})\{\|\mathbf{x} - \mathbf{x}_c^k\| - r^k\} \qquad (3)$$

And the enrichment function $\psi^k(\mathbf{x})$ can be chosen such as:

$$\psi^k(\mathbf{x}) = \sum_i |\phi_i^k| N_i(\mathbf{x}) - \left| \sum_i \phi_i^k N_i(\mathbf{x}) \right| \qquad (4)$$

This enriched approximation eliminates all the numerical artefacts exhibited for nearby inclusions in the classical XFEM/level-set method.
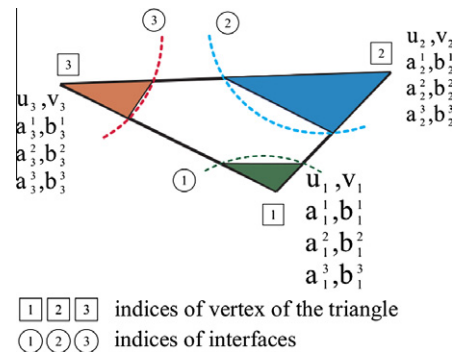

Fig. 3. μ-XFEM method principle illustrated in a simple 2D case with three inclusions intersecting an element.
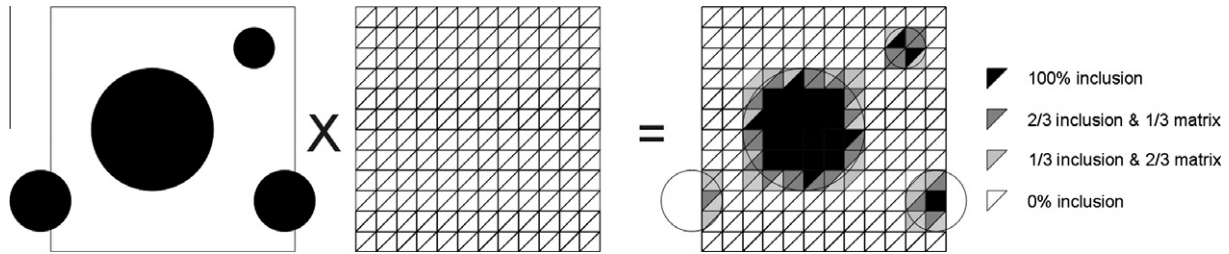
Fig. 4. BENHUR method principle illustrated for a simple 2D mesh with four inclusions.

3.4. Fuzzy projection of the microstructure on meshes or regular grids

3.4.1. Benhur Preprocessor

BENHUR is a preprocessor used to attribute homogenised properties to elements lying across inclusions and matrix [34]. It is used to improve the results obtained on meshes which are not constrained to follow the geometry of the elements. this treatment a practical approach when used in conjunction with numerical methods such as FFT solvers and finite differences which are very efficient but require Cartesian grids.

The volume fraction (f_i, resp. f_m) of each phase in elements where overlaps occur is estimated statistically using a large number of test points. The behaviour associated to each element is then derived from a number of possible homogenisation procedures (as illustrated in Fig. 4). The procedures implemented and tested for the purpose of this benchmark are (p is the physical property considered):

- Hill inf: $p = \min(p_i, p_m)$.
- Hill sup: $p = \max(p_i, p_m)$.
- Voigt: $p = f_i p_i + (1 − f_i)p_m$.
- Reuss: $p = 1/(f_i/p_i + (1 − f_i)/p_m)$.
- "FFT" $p = p_i$ if $f_i > 0.5$, $p = p_m$ otherwise.

The "FFT" homogenisation method is called that way because it is the default method for FFT solvers. BENHUR was used in the context of this benchmark with an FEM solver, an FFT solver and a finite difference grid. Here, we test the combination of preprocessor and numerical discretisation.

3.4.2. Solvers used in conjunction with BENHUR

The FFT method was originally proposed by Moulinec and Suquet [35], and the version used for this benchmark is the *accelerated scheme augmented Lagrangian* as described by Moulinec and colleagues [36]. The convergence of this method is strongly dependent on a reference elastic tensor. However this tensor is not very sensitive to mesh refinement. Therefore, it is optimised for a coarse mesh of 64^3 voxels. As a verification, the alternative discretisation of the Green function proposed by Willot and Pellegrini has also been used to compute the effective properties of the concrete microstructure [37]. No significant difference in convergence properties was observed. The solver used was *morph-hom*.[4] Problems with up to 1024^3 voxels were solved using a 12-cores 2.7 GHz Xeon computer with 96 GB of RAM. A seven node cluster was used to obtain further results with 2184^3 and 2268^3 voxels.

Cartesian grids are also suitable for computations using finite difference or finite volumes schemes. Such schemes are more memory-efficient than finite elements and are suitable for transport problems. An implicit central difference scheme was implemented, leading to a 7-band sparse matrix. This well-structured matrix could then be solved efficiently using a incomplete-Cholesky preconditioned conjugate gradient method. This highlights a central advantage of the BENHUR method, which it owes to its applicability to structured grids. In the case of finite volume method the BENHUR preprocessor has been used to determine the property of the cell centred scheme and then solved with a multi-grid approach.

To provide an overview of the different methods, their essential features have been summarised in Table 5.

4. Results and discussion

4.1. Results

The apparent properties obtained as a function of the numerical method and mesh fineness are plotted in Figs. 5 and 6. On the y-axis is the absolute value of the apparent property, and on the x-axis is h the average characteristic length of the elements. The bounds on the y-axis go from 50% to the final value of the FFT computations to 200% when possible. Thus, all the graphs lie within comparable bounds in order to make the comparison of the methods possible.

A number of effects are visible on these graphs. The first visible effect is that when inclusions have large values of their mechanical or thermal properties relative to the matrix this results in larger divergence of the simulated values for coarse meshes. This effect is visible both in the thermal and the mechanical simulations. Notably, there is a larger divergence in the conduction and mechanical cases for contrasts of 10^2 than when the contrast is $10^{−2}$ or $10^{−8}$. Fig. 7 highlights the similarity of the contrast = 10^2 behaviour in the thermal and mechanical simulations. The second effect is that complex geometries cause larger divergences in coarse meshes. Indeed, the error for the B11 and B3200 cases are significantly larger than in the octahedron and sphere benchmarks. The third effect is that numerical methods based on Cartesian grids are stiffer than methods using conforming meshes. Both the FFT and the XFEM approach seem to converge towards larger apparent values than CAST3M or AMIE.

Another remarkable result is that the apparent property does not converge to the same value independent of the numerical method. This goes against physics and it seems that due to the specific layout of the mesh used, a bias is introduced. As AMIE does not mesh the smaller inclusions explicitly, the resulting mesh can be stiffer of softer depending on where the elements lie with respect to the microstructure geometry. The quadratic AMIE meshes are also softer as the intermediate points are projected on the surfaces of the inclusions. This reduces considerably the geometrical error when the microstructural boundaries are curved; however, it modifies slightly the phase fraction compared to CAST3M.

In most cases, the results from the Neumann and Dirichlet boundary conditions define the upper and lower bounds for the results obtained with periodic conditions. This is however not the

---

[4] By MINES-PARISTECH.

Table 5

Overview of the different methods and how they differ in terms of behaviour attribution: per elements or per Gauß point, whether the behaviours are taken from phases presents or computed as mixtures; the kind of elements used; the kind of mesh used.

| Method	Boundary conditions	Mesh type	Behaviour attribution	Choice of shape functions
CAST3M	Dirichlet/Neumann	Conforming	Element location	– lin. Lagrangian
AMIE	Dirichlet/Neumann	Conforming[a]	Element location	– lin. Lagrangian – quad. Lagrangian
μ-XFEM	Dirichlet/Neumann	Cartesian	Gauß points location	– lin. Lagrangian – enriched
BENHUR + FV	Dirichlet/Neumann	Cartesian	hom. mixture from feature overlap	– lin. Lagrangian
FFT	Periodic	Cartesian	Largest featureoverlap	FFT
BENHUR-FFT	Periodic	Cartesian	Hom. mixture from feature overlap	FFT

[a] When mesh density allows it.
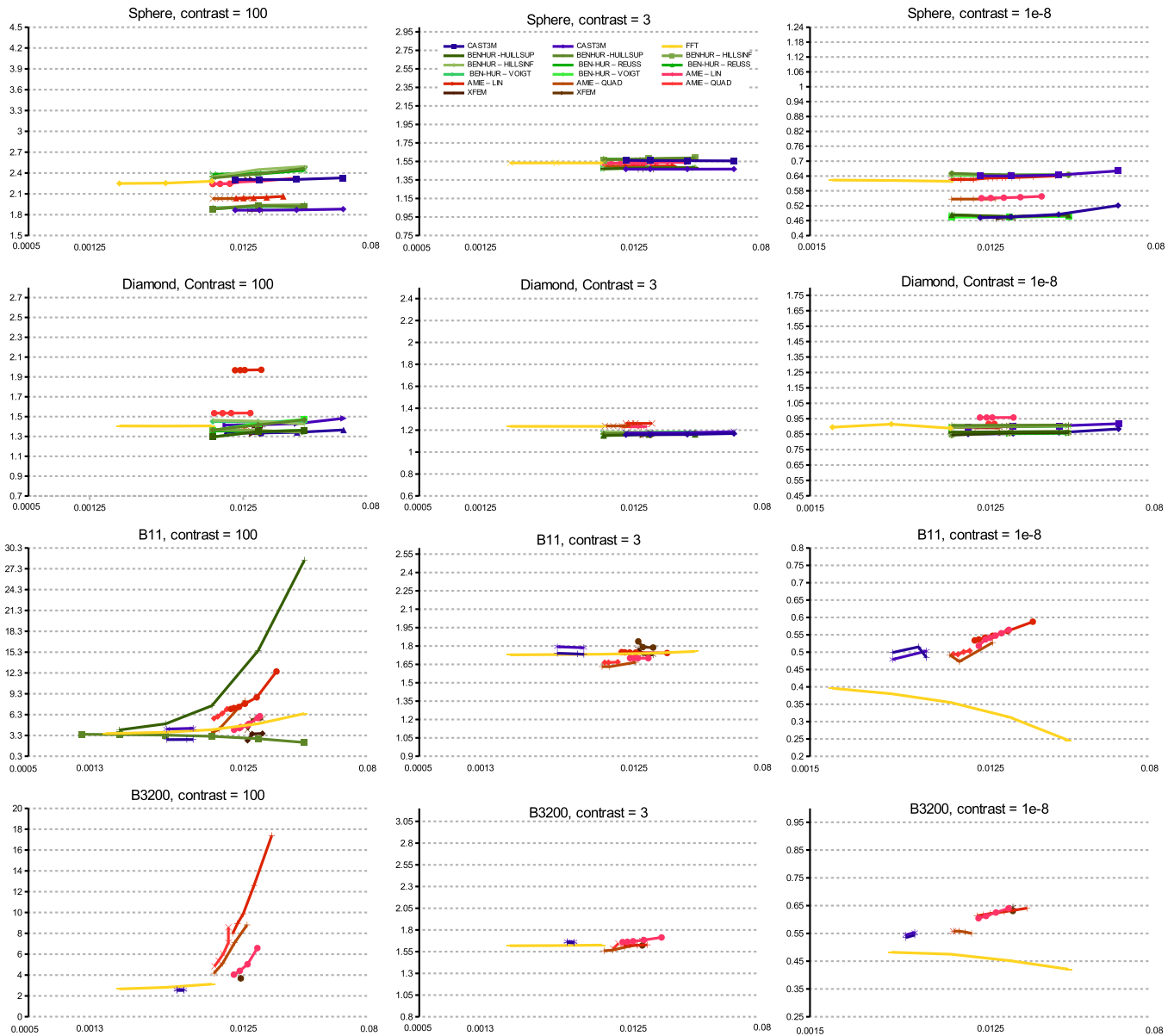
Fig. 5. Apparent mechanical properties (C_{1111}) of the different geometries modelled. On the *x*-axis is *h*, the characteristic element size.

case in the B3200, thermal contrast = 0.01 case, nor in the B11 and B3200 mechanical contrast = 10^{-8} cases. In these cases, the large number of soft inclusions bias the results from the FFT which is significantly softer than it should be. Indeed, in these cases, values are approximated from below. This is probably due to the fact that many elements have a phase content of more than 50% inclusion and therefore have the behaviour of the inclusion which results in a very soft mesh. Finally, when comparing the results from Dirichlet and Neumann boundary conditions, the results are notably closer in the B3200 compared to B11. This is probably due to
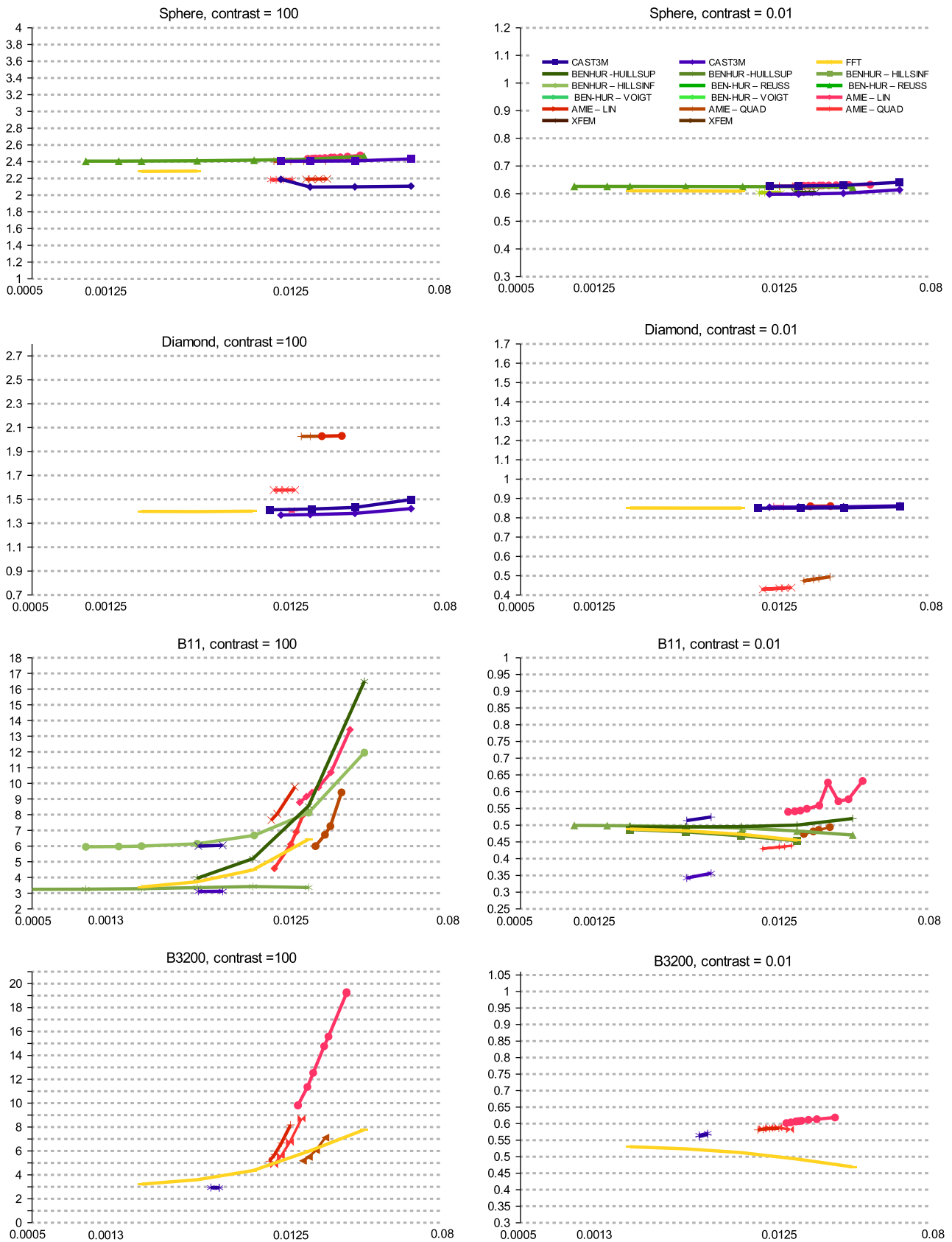
Fig. 6. Apparent thermal properties (λ_{11}) of the different geometries modelled. On the x-axis is h, the characteristic element size.

the heterogeneity of the microstructure at the boundaries in the B11 case: large phase contrasts on the surfaces where stresses are applied result in larger distortions.

The effect of the stress concentrators in the octahedron case are particularly visible: as the discretised geometry produced by AMIE has sharp edges, large stresses or temperature gradient are in-
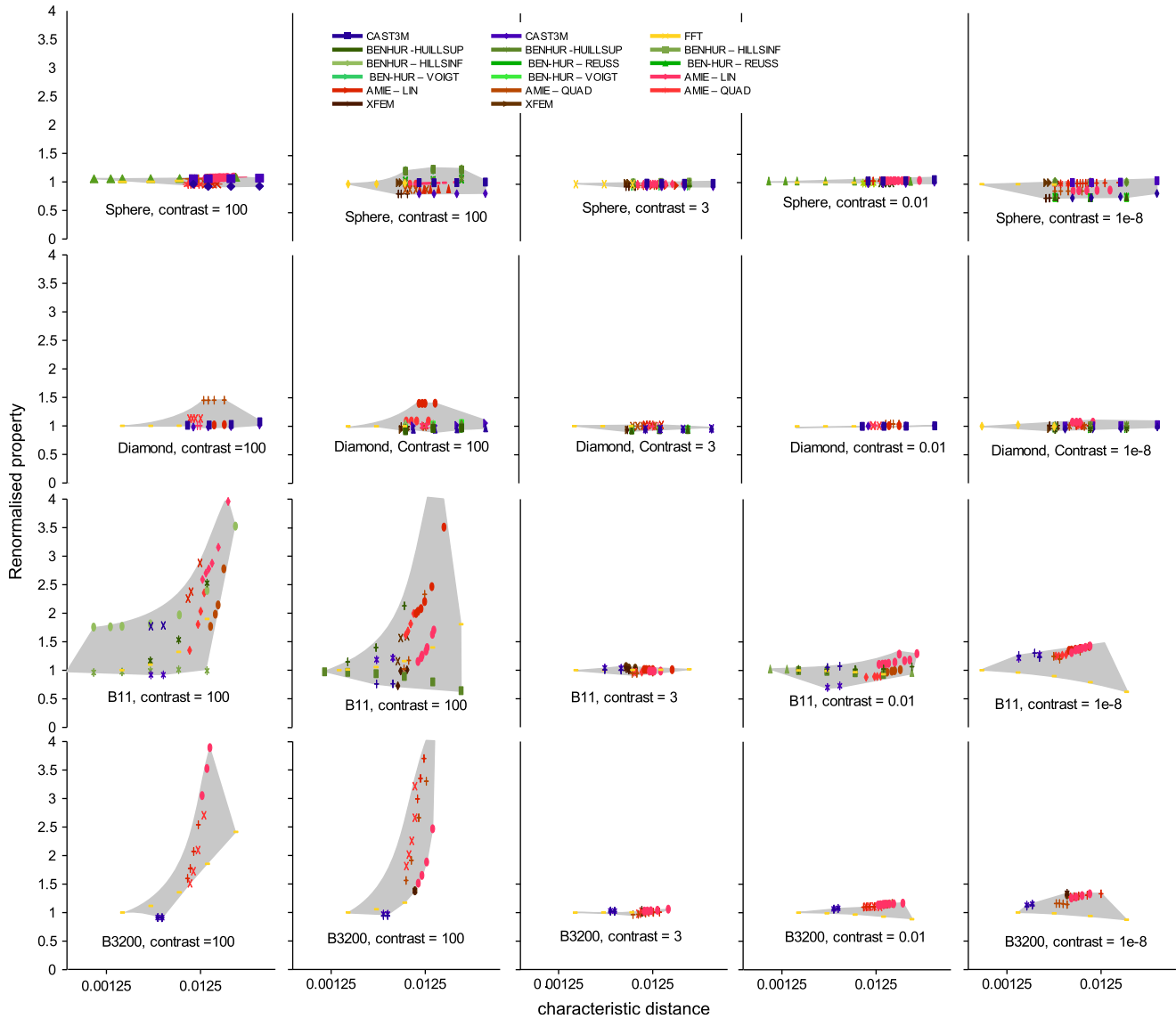
Fig. 7. Outlined behaviour of the various methods. The values of the apparent properties have been normalised to the final value obtained with FFT. This figure highlights the dispersion of the results as a function of geometry and contrast. The first contrast = 10^2 column is thermal and the second mechanical. On the *x*-axis is *h*, the characteristic element size.

duced. The apparent properties become then significantly larger in the contrast = 100 case.

4.2. Error minimisation and convergence

The benchmark proposed in the article helped identify which numerical strategies best alleviate different error types. The first cause of error is the mis-representation of geometry. Finite element meshing with conforming meshes and linear elements always yield a lower inclusion fraction compared to the input geometry if it is convex and curved. This is because the curved external boundaries of inclusions are formed by tesselating these surfaces with triangles. The geometry-based error grows in the case of smaller inclusions and small inter-inclusion distance, represented by fewer elements. For a fixed number of discretisation points, representing these inclusions with a very small number of nodes is preferable to not representing them at all. Even when the inclusions are not meshed, giving some elements the behaviour of the inclusion causes the phase fraction to be better approxi-

mated. The μ-XFEM produces an always better representation of geometry, although a very coarse Cartesian base grid will yield a somewhat imprecise description of the geometry, due to the multiple level-set approximation. BENHUR hardens or softens the elements overlapping phases. The choice of the homogenisation technique used to determine the inter-phase elements must be done as a function of the problem. In general however, the Voigt and Reuss methods seem to be the better choices and converge significantly faster than those based on the Hill bounds.

A second type of error comes from insufficient element density in regions where large gradients need to be captured. The FEM provides the most control to limit this error, using appropriate heuristics for mesh density. Unfortunately, this is at the cost of larger problems. The XFEM method is very sensitive to this kind of errors, as it uses an underlying Cartesian grid. The order of the elements of that grid limits the gradients that can be captured. Thus, although the error is initially very low, even for very coarse meshes, the convergence is slow, as further improvement only come from the finer discretisation of the problem. Furthermore,

the number of degrees of freedom per node is significantly larger than in the case of the other methods.

The third type of error, which is very important in conduction problems is the connectivity error. Artificial connections between inclusions can be formed due to meshing errors. When these errors dominate, the μ-XFEM is the most appropriate tool, as it can eliminate them completely. AMIE's meshing heuristic also limits these errors, at the cost of making an error on the inclusion fraction. BENHUR approximates connections which have not been meshed by using elements whose properties have been obtained through a local homogenisation rule. Whether the bulk of the error comes from artificial connectivity or from surface approximations depends on the scheme chosen.

The convergence behaviour of the various numerical methods is plotted in Figs. 8 and 9. The value which is plotted is the relative error within each series; the error is computed as (ν the apparent property):

$$\epsilon_i = \left| \frac{\nu_i - \nu_{\text{finest}}}{\nu_{\text{finest}}} \right| \tag{5}$$

The error cannot be absolute as the "converged" value is not known for all series, and in any case, can be different depending on the numerical scheme used. However, the relative error measure can be usefully used to assess the asymptotic convergence rate of the different methods.

In general, these observations show that there are two components to the asymptotic behaviour of the numerical value of the error ε.

$$\varepsilon = C\mathcal{O}(h^n) \tag{6}$$

One component (C) is the part which comes essentially from the mis-representation of geometry, notably in the case of the concrete and mortar microstructures, the connections between pores or inclusions. As this is always correct in the case of μ-XFEM, the initial error is low. Methods using Cartesian grids have a high C, but can compensate by using significantly smaller elements as the memory cost of storing the mesh is much lower. The other component of the error (h^n) comes from the approximation of the solution due to the choice of fields and the size of the elements h. n is the order of the convergence. When the results are computed on Cartesian grids,
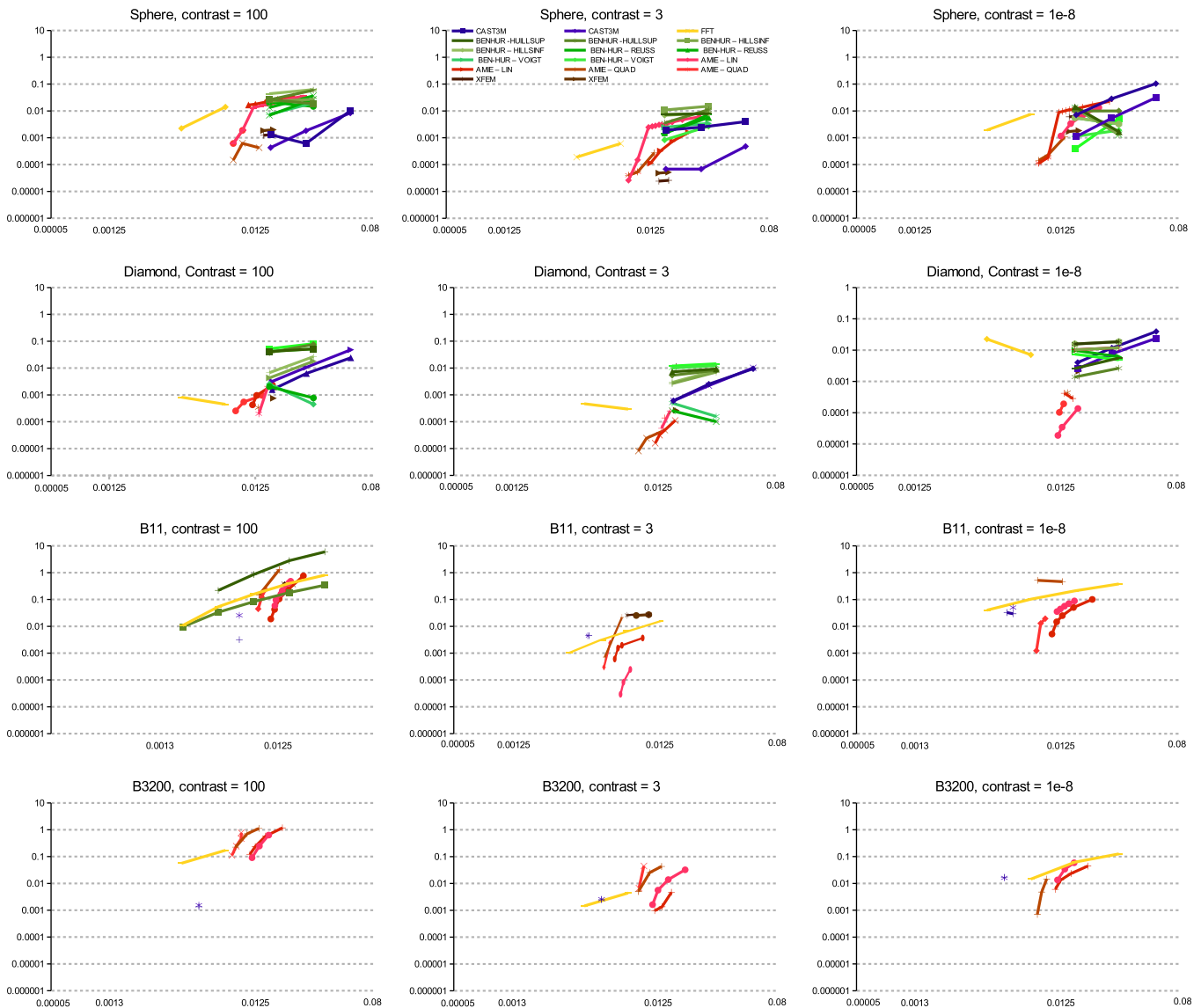

Fig. 8. The apparent relative error for each series is plotted. These are mechanical problems. When a series has a single result, it is not plotted. When a series has only two values, the slope cannot be inferred. On the x-axis is h, the characteristic element size.
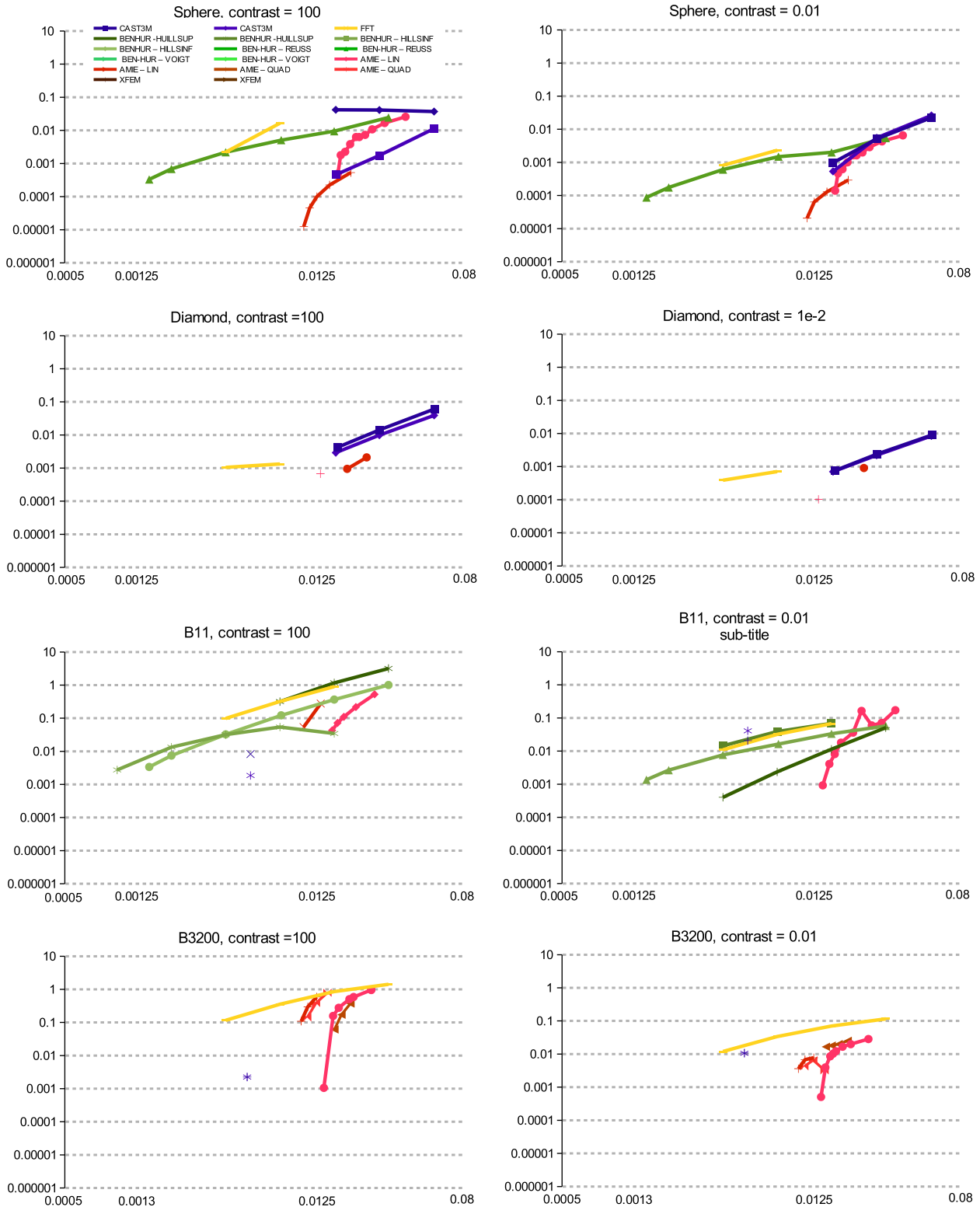
Fig. 9. The apparent relative error for each series is plotted. These are steady-state diffusion problems. When a series has a single result, it is not plotted. Series with single results were not plotted. On the *x*-axis is *h*, the characteristic element size.

large gradients of stresses of concentration cannot be well captured as fields vary linearly or quadratically over elements which are not oriented in the direction of the maximum gradient. The methods using conforming fields, CAST3M and AMIE have the higher convergence slope due to the closer-to-optimal placements of the elements. AMIE has the highest convergence rate as the mesh simultaneously converges to the exact geometry as well as becoming finer.

4.3. Estimation of effective properties

The strengthening theorem [38] explains why finite element-based approaches overestimate the apparent mechanical or thermal properties, this is because the choice of shape functions in finite elements always yields a solution with lower elastic energy than the solution corresponding to the real displacement field

Table 6

Overview of the advantages and flaws of the methods presented in this work. Heuristic meshing improves on FEM by allowing coarse meshes, which could not have been generated had conformance been required. XFEM improves over FEM by having an always perfect representation of geometry—provided it has no sharp angles. BENHUR can be used in conjunction with very fast solvers, but requires the choice of appropriate homogenisation schemes for each problem.

	Conforming FEM	AMIE	μ-XFEM	BENHUR + FEM	BENHUR + FFT
Coarse mesh precision	–	+	++	–/+	–/+
Medium mesh precision	–	++	+++	+/++	+/++
Fine mesh precision	+++	+++	+++	++/+++	+++
Max precision	++	++	++	++	+++
Speed	+	++	+	++	+++
Genericness	+++	+++	++	–	–
Sharp geometries	+++	+++	–	+	+

[39]. Only the BENHUR preprocessor will underestimate properties in certain cases, due to sampling or from the local homogenisation producing too-soft elements. In all cases convergence to a final apparent property was observed, but excessive errors for rough discretisations and high contrasts were observed: up to 400% in the case of the concrete-like materials, B11 and B3200. This confirms the observation which prompted the development of the techniques described in this paper, namely that microstructural simulation, even in the case of linear diffusion or elasticity, is a hard numerical problem in the case of complex geometry.

As all methods need fine grids to provide adequate apparent properties, the Cartesian grid based methods with the BENHUR preprocessor have an advantage as they yield matrices which can be stored very effectively—or in the case of finite differences, not stored at all. However, they require the choice of an appropriate local homogenisation scheme, which is not easy to pick: significant differences were observed in the final values depending on the choice of scheme. Table 6 gives a summary of the strengths and weaknesses of each method. In this table the "genericness" character describes how much this method is directly applicable to different problems or whether it needs application-specific tweaks.

5. Conclusion

The methods presented in this paper do not form an exhaustive list of possibilities, and more methods can be found published in the literature. However, they represent varied attempts at alleviating the various sources of error inherent in the simulation of reconstructed microstructures, and effectively span the range of methods which are commonly encountered. Therefore, taken together, they can be used to formulate recommendations about what is the best numerical strategy to apply, depending on the type of numerical difficulties encountered. Table 6 provides a qualitative summary of the advantages and disadvantages of the methods. The methodology described in this paper that was used to compare them was found useful and highlighted strengths and weaknesses which were not obvious.

In the case of complex microstructures where the main difficulty consists in capturing the effects cased by closely packed particles, where the error will mostly come from artificial contacts, XFEM is a good candidate at low number of elements. For larger numbers of elements, relaxed meshing will allow the production of meshes which give good approximations at moderate computing costs. If yet more computing power available, good estimates can be produced using BENHUR or the classical finite element method. If the constituents of the geometry are not closely packed but well-separated, BENHUR gives good approximations at low mesh densities. In the case of simple geometries with well-defined edges, the classical finite element method should be preferred, as it gives very good results, even for very coarse meshes. In the case of simple geometries with curved surfaces, quadratic elements should be used as they significantly reduce the geometrical error. Finally, when an FFT solver can be used, very good approximations can be had in all cases as extremely fine meshes can be considered. In the latter case, preprocessing using BENHUR can improve the results, provided that enough is known that an appropriate homogenisation scheme can be chosen.

The significant differences observed between the methods show that for complex geometries, reliably obtaining apparent linear properties for high phase contrasts is a difficult problem which merits further attention. The results are shown here for simplified 2-phase materials, but the wide range of phase contrasts described makes them applicable to more realistic representation of cementitious composites.

References

[1] Escoda J, Willot F, Jeulin D, Sanahuja J, Toulemonde C. Estimation of local stresses and elastic properties of a mortar sample by fft computation of fields on a 3d image. Cem Concr Res 2011;41(5):542–56.

[2] Salmi M, Auslender F, Bornert M, Fogli M. Apparent and effective mechanical properties of linear matrix-inclusion random composites: improved bounds for the effective behavior. Int J Solids Struct 2010;49(10):1294–303.

[3] Mori T, Tanaka K. Average stress in matrix and average elastic energy of materials with misfitting inclusions. Acta Met 1973;21:571–4.

[4] Kröner E. Berechnung der elastischen konstanten des vielkristalls aus den konstanten des einkristalls. Zeitschrift Für Physik A Hadrons and Nuclei 1958;151(4):504–18.

[5] Torquato S. Random heterogeneous materials. Microstructure and macroscopic properties. Springer; 2001.

[6] Zohdi TI, Wriggers P. Introduction to computational micromechanics. 2nd reprinting ed. Springer-Verlag.

[7] Idiart MI, Willot F, Pellegrini YP, Castañeda PP. Infinite-contrast periodic composites with strongly nonlinear behavior: effective-medium theory versus full-field simulations. Int J Solids Struct 2009;46(18):3365–82.

[8] Huet C. Coupled size and boundary condition effects in viscoelastic heterogeneous bodies. Mech Mater 1999;31(12):787–829.

[9] Kanit T, Forest S, Galliet I, Mounoury V, Jeulin D. Determination of the size of the representative volume element for random composites: statistical and numerical approach. Int J Solids Struct 2003;40(13):3647–79.

[10] Schlangen E, Van Mier JGM. Simple latice model for numerical simulation of fracture of concrete materials and structures. Mater Struct 1992:534–42.

[11] Wang ZM, Kwan AKH, Chan HC. Mesoscopic study of concrete i: generation of random aggregate structure and finite element mesh. Comput Struct 1999:533–44.

[12] Zohdi TI, Wriggers PE. Aspects of the computational testing of the mechanical properties of microheterogeneous material samples. Int J Numer Method Eng 2001;50:2573–99.

[13] Wriggers PE, Moftah SO. Mesoscale models for concrete: homogenisation and damage behaviour. Finite Elem Anal Des 2006;42:623–36.

[14] Comby-Peyrot I, Bernard F, Bouchard P-O, Bay F, Garcia-Diaz E. Development and validation of a 3d computational tool to describe concrete behaviour at mesoscale. application to the alkali-silica reaction. Comput Mater Sci 2009;46:1163–77.

[15] Vorel J, Smilauer V, Bittnar Z. Multiscale simulations of concrete mechanical tests. J Comput Math 2012 [p. online].

[16] Gitman IM, Askes H, Sluys LJ. Representative volume: existence and size determination. Eng Fract Mech 2007;75(16):2518–34.

[17] Dunant CF, Scrivener KL. Micro-mechanical modelling of alkali–silica-reaction–induced degradation using the amie framework. Cem Concr Res 2010;40:517–25 [4].

[18] Hain M, Wriggers PE. Computational homogenization of micro-structural damage due to frost in hardened cement paste. Finite Elem Anal Des 2008;44(5):233–44.

[19] Cascon JM, Kreuzer C, Nochetto RH, Siebert KG. Quasi-optimal convergence rate for an adaptive finite element method. SIAM J Numer Anal 2008;46(5):2524–50.

[20] Zohdi TI. Modeling and simulation of a class of coupled thermo-chemo-mechanical processes in multiphase solids. Comput Methods Appl Mech Eng 2004;193(6):679–99.

[21] Sanahuja J, Toulemonde C. Numerical homogenization of concrete microstructures without explicit meshes. Cem Concr Res 2011;41:1320–9.

[22] Bary B, Ben Haha M, Adam E, Montarnal P. Numerical and analytical effective elastic properties of degraded cement pastes. Cem Concr Res 2009:902–12.

[23] Rupp I, Peniguel C, Tommy-Martin M. Large scale finite element thermal analysis of the bolts of a french pwr core internal baffle structure. Nucl Eng Technol 2009;41(9).

[24] Rupp I, Peniguel C. Coupling heat conduction, and convection in complex geometries. Int J Numer Methods Complex Geometries, Methods Heat Fluid Flow 1999;9.

[25] Dunant CF. Experimental and modelling study of the alkali–silica-reaction in concrete. PhD thesis; 2009.

[26] Dunant CF, Vinh PN, Belgasmia M, Bordas S, Guidoum A. Architecture tradeoffs of integrating a mesh generator to partition of unity enriched object-oriented finite element software. Revue Européenne de Mécanique Numérique 2007;16:237–58.

[27] Dunant CF, Kerfriden P, Bordas S, Scrivener KL, Rabczuck T. An algorithm to compute damage from load in composites. Front Archit Civil Eng China 2011;5(2):180–93.

[28] Belytschko T, Parimi C, Moës N, Sukumar N, Usui S. Structured extended finite element methods for solids defined by implicit surfaces. Int J Numer Method Eng 2003;56:609–35.

[29] Fries TP. A corrected xfem approximation without problems in blending elements. Int J Numer Method Eng 2008;75(5):503–32.

[30] Gracie R, Wang H, Belytschko T. Blending in the extended finite element method by discontinuous galerkin and assumed strain methods. Int J Numer Method Eng 2008;74(11):1645–69.

[31] Moës N, Cloirec M, Cartraud P, Remacle J-F. A computational approach to handle complex microstructure geometries. Comput Methods Appl Mech Eng 2003;192(29):3163–77.

[32] Sukumar N, Chopp DL, Moës N, Belytschko T. Modeling holes and inclusions by level-sets in the extended finite-element method. Int J Solids Struct 2001;190:6183–200.

[33] Tran AB, Yvonnet J, He Q-C, Toulemonde C, Sanahuja J. A multiple level-set approach to prevent numerical artefacts in complex microstructures with nearby inclusions within xfem. Int J Numer Method Eng 2011:1436–59.

[34] Toulemonde C, Masson R, Gharib JE. Modeling the effective elastic behavior of composites: a mixed finite element and homogenisation approach. Comptes Rendus Mécanique 2008;336:275–82.

[35] Moulinec H, Suquet P. A fast numerical method for computing the linear and nonlinear mechanical properties of composites. Comptes Rendus Mécanique 1994;318:1417–23.

[36] Michel J-C, Moulinec H, Suquet P. A computational scheme for linear and non-linear composites with arbitrary phase contrast. Int J Numer Method Eng 2001;52:139–60.

[37] Willot F, Pellegrini YP. Fast fourier transform computations and build-up of plastic deformation in 2d, elastic-perfectly plastic, pixelwise disordered porous media. In: Jeulin D, Forest S, editors. Continuum models and discrete systems CMDS 11. Paris: École Des Mines; 2008. p. 443–9.

[38] Hill R. Elastic properties of reinforced solids: Some theoretical principles. J Mech Phys Solids 1963;11:357–72.

[39] Liu GR, Nguyen TT, Dai KY, Lam KY. Theoretical aspects of the smoothed finite element method (SFEM). Int J Numer Method Eng 2007;71(8):902–30.